

EFFECT OF CHEMICAL COMPOSITION AND T6 HEAT TREATMENT ON THE MECHANICAL PROPERTIES AND FRACTURE BEHAVIOUR OF Al-Si ALLOYS FOR IC ENGINE COMPONENTS

D. Vuksanović, V. Asanović, J. Šćepanović, D. Radonjić*

University of Montenegro, Faculty of Metallurgy and Technology, Podgorica, Montenegro

(Received 10 May 2019; Accepted 20 January 2021)

Abstract

The microstructural examinations of Al-Si alloys intended to manufacture IC engine components revealed a complex phase composition in all the samples. The polyhedral crystals of primary silicon were detected in the Al-12.5Si alloy, besides the α -Al phase, eutectic silicon, and several intermetallic phases, identified in the cast samples of both alloys. Better tensile properties were found for the samples of Al-11Si. A predominantly intercrystalline fracture with features of ductile failure was observed in both alloys. In as-cast specimens of the Al-11Si alloy, the cracks were formed by the decohesion mechanism between the particles of the intermetallic phase AlCuFeNi and the α -Al phase. The microcracks initiated on the interface were spread along the branches of the α -Al₃(Fe,Mn,Cu)₃Si₂ particles. After T6 treatment of the Al-11Si alloy, almost half of the intermetallics quantity presented the Al₃Ni phase, while the iron-based phases were observed in a small amount. Spheroidized eutectic silicon, a smaller portion of Al₅Cu₂Mg₈Si₆, and a more considerable quantity of Al₃(Fe,Mn,Cu,Ni,Co) were detected for T6 specimens of the Al-12.5Si alloy. The rounded crystals of eutectic silicon contributed to the improvement of their tensile properties. Larger and deeper dimples of mostly polygonal shapes were observed in the samples of the Al-11Si alloy after T6 treatment. The microcracks occurred at the boundary of the intermetallic phase/ α -Al solid solution.

Keywords: Intermetallic phases; Mechanical properties; Fracture

1. Introduction

Aluminium-silicon alloys have been recognised for a long period of time as the essential material in automotive, transportation, and several other industries [1]. Aside from their excellent castability, good corrosion resistance, and low specific gravity [2], those alloys exhibit a high strength to weight ratio as well as an excellent thermal conductivity [3]. Nowadays, aluminium-silicon castings widely substitute the cast iron for manufacturing the engine components [3]. Designing of Al-Si alloys with a good combination of castability and plasticity is based on the silicon concentration defined in the range from 4 % to 22 % [4]. Those materials are generally classified according to their silicon content into three major groups: hypoeutectic (below 12 %), eutectic (12 % - 13 %), and hypereutectic (14 % - 25 %) [5]. The alloys containing about 50 vol. % to 90 vol. % of the eutectic phase are mostly used in the automobile industry [6, 7]. The primary purpose of the hypoeutectic alloys is the manufacturing of the engine blocks, cylinder heads, and wheels [8]. The

hypereutectic Al-Si alloys find application in cylinders, cylinder liners, cylinder heads, air compressor cylinders, engine pistons, pumps, and piston rings [9-12]. Hard primary silicon crystals provide superior wear resistance of hypereutectic alloys but also reduce tool life in machining process [9]. In order to achieve favourable wear performance and simultaneously minimise issues related to the tool life, it is necessary to ensure small particles of primary silicon uniformly distributed in the matrix of the aluminium [9].

Alloying elements which have strengthening effects such as magnesium, nickel, copper, and zinc are usually added to Al-Si alloys for the purpose of improving their mechanical, physical, and service properties [13]. Transition elements such as iron, manganese, and chromium are commonly found impurities in aluminium [14]. Different intermetallic phases depending on chemical composition and production process may be formed in Al-Si alloys. Hence, the phases such as Al₂Cu, Mg₂Si, Al₂CuMg, silicon as well as Al(Fe,M)Si, where M denotes manganese, vanadium, chromium, molybdenum or

Corresponding author: draganra@ucg.ac.me

<https://doi.org/10.2298/JMMB190510014V>



copper could be expected in the alloys' microstructures. [15]. Good precipitation hardening effects are guaranteed by a copper level between 2 % and 4 % [13]. The strength and hardness of Al-Si alloys at elevated temperatures may be improved by the addition of nickel [14], and its typical content is up to 2 wt. % in pistons intended for artificial ageing [13]. The reduction in the tensile strength of Al-Si-Mg alloys was found with increasing of the silicon content over 16 %, while ductility was decreased with the change of the silicon concentration from 4 % to 20 % [16]. The T6 heat treatment is usually used for enhancing the mechanical properties of the Al-Si alloys [1, 17]. The slight improvement of the tensile strength of heat-treated (T5 or T6) castings made from Al-Si alloys is achieved by the addition of 1 wt.% to 4 wt.% of zinc [13]. Han et al. [17] observed that the tensile properties of Al-Si-Cu-Mg 319 alloy depended on the distribution of Al_2Cu , incipient melting of $Al_5Cu_2Mg_8Si_6$ and Al_2Cu phases, as well as the characteristics of silicon particles.

Minor alloying elements such as strontium, titanium, boron, phosphorus, and rare earth elements are added to Al-Si alloys to improve their mechanical properties and service characteristics [13]. The size and morphology of eutectic silicon in hypoeutectic and eutectic Al-Si alloys are governed by chemical modification [9] which is based on the introduction of a small amount of sodium, strontium, calcium, and antimony to those alloys [8, 18]. Although an effective modification may be achieved by the addition of a small quantity of strontium, the commonly used content is between 0.008 % and 0.04 % [19].

Iron as a typical impurity in Al-Si casting alloys may form different phases, but a needle-shaped β - Al_3FeSi phase, especially the one that appeared during solidification as a primary crystal, has the most harmful effect on their mechanical properties [4]. Cobalt, molybdenum, chrome, nickel, and beryllium are added to Al-Si alloys to promote the formation of α - $Al_{15}Fe_3Si_2$ instead of β - Al_3FeSi [20]. Wang and Xiong [21] reported that the change of the morphology of iron-rich phases from needles or plates to Chinese scripts or polygons was caused by the addition of beryllium to Al-Si-Mg-Ti cast alloys. Farahany et al. [22] observed a significant increase in tensile properties of Al-Si-Cu-Zn alloy containing strontium compared to the similar alloys in which bismuth and antimony were added. Karamouz et al. [23] found that the addition of lithium to Al-Si-Cu-Fe alloys modified β - Al_3FeSi effectively, but led to the porosity of castings. Tzeng et al. [24] studied the influence of scandium addition on iron-bearing phases in Al-Si-Mg alloys. It was declared that the acicular β - Al_3FeSi phase was transformed into small nodular $Sc-Fe(Al_{12}Si_6Fe_2(Mg,Sc)_5)$ phase leading to the

improvement of the ductility of Al-Si-Mg alloys [24].

The raising of operational parameters and performance of IC engine parts must be solved by designing materials with microstructure and mechanical properties which could satisfy technological requirements for manufacturing at an acceptable economic level [25]. Many parts of automotive engines are subjected to the elevated temperatures during the service. Therefore, numerous examinations have been performed to design chemical composition which enables improvement of mechanical properties and ductility [1, 16, 24, 26-28, 29-32], good deformation resistance [27, 33-35] as well as wear behaviour [36-39]. This research is aimed at developing the Al-Si alloys reliable in the service. The alloys were designed as hypoeutectic with 10.93 % of silicon and hypereutectic containing 12.50 % of silicon. The weight ratio of Cu/Mg was planned as 1.1 in the hypoeutectic and 1.6 in the hypereutectic alloys. A similar content of nickel, iron, cobalt, and manganese was chosen, while the concentration of molybdenum was quite different. The microstructure, mechanical properties and fracture behaviour of multicomponent Al-Si alloys was studied in as-cast and T6 heat-treated samples.

2. Experimental procedure

Two alloys Al-11Si and Al-12.5Si used in this study were prepared by melting AlSi10Mg master alloy, pre-alloys (Al-33% Cu, Al-60% Mn, and Al-75% Fe), technically pure silicon, nickel and molybdenum in a 20-kW electric resistance furnace using a graphite crucible. The melting temperature was kept at $780\text{ }^\circ\text{C} \pm 5\text{ }^\circ\text{C}$. The TAL-2 consisting of potassium chloride, sodium chloride, and cryolite reacting at $690\text{ }^\circ\text{C}$ was added for the fluxing melts in the amount of about 2 % of the quantity of each melt. The degassing of molten Al-Si alloys was performed by Hexachloroethane tablets in the amount approximately equal to 0.25% of their quantity. The Al-10% Sr master alloy was added to the melts for the modification of eutectic silicon. The alloys were poured at $740\text{ }^\circ\text{C} \pm 5\text{ }^\circ\text{C}$ into the permanent grey cast iron moulds which had not been preheated previously. After the solidification, the castings were removed from the moulds and further cooled down to room temperature. The chemical composition of the produced alloys is listed in Table 1. The T6 heat treatment was performed to achieve high strength, necessary for the application conditions of engine pistons [27, 40] although an increase in tensile strength may be accompanied by a decrease in elongation [4]. The alloys were solution treated at $520\text{ }^\circ\text{C} \pm 5\text{ }^\circ\text{C}$ for 6 hours followed by quenching in water (at $70\text{ }^\circ\text{C}$) as shown in Figure 1. The subsequent



ageing treatment was performed at $205\text{ }^{\circ}\text{C} \pm 5\text{ }^{\circ}\text{C}$ for 7 hours while specimens were finally cooled in ambient air.

The tensile test specimens with 4.0 mm gauge diameter and 45.0 mm gauge length were prepared from the as-cast and T6-treated alloys. The machine 1195 Instron was used for the determination of the tensile strength and relative elongation of the samples at room temperature, while the testing machine produced by Karl Frank GmbH, type 38532 was applied for measuring their hardness as Brinell hardness HB 5/250/30. The microstructures of as-cast and T6-treated specimens were revealed by an optical microscope and scanning electron microscope JEOL JSM-6460 LV, equipped with an energy dispersive X-ray spectroscopy. The fractured samples of as-cast and T6-treated alloys were observed using JEOL JSM-6460 LV in secondary electron mode in order to study the fracture behaviour of alloys.

3. Results and discussion

3.1. Microstructural characterisation

The complex phase composition was revealed during microstructural examinations of the as-cast and T6-treated specimens of Al-Si alloys, as shown in Table 2. The optical micrographs of examined alloys are shown in Figures 2, 4, 6, and 7, and corresponding SEM-EDS spectra from the α -Al phase, silicon particles, and intermetallic phases are presented in Figures 3 and 5. Almost 71 vol. % of α -Al phase, 21 vol. % of eutectic silicon, and around 8 vol. % of several intermetallic phases were found in as-cast samples of Al-11Si alloy (Table 2). Coarse dendrites of α -Al phase were unevenly distributed within the cross-section of the as-cast samples of hypoeutectic Al-11Si alloy. While the directional growth of α -Al dendrites was observed in the surface of the specimen (Figure 2a), in its central part, several small areas without primary α -Al crystals around the porosity could be recognised (Figure 2b), indicating higher cooling rate during crystallisation. Modified eutectic silicon with significantly diverse morphology formed a fine mixture with $\text{Al}_5\text{Cu}_2\text{Mg}_8\text{Si}_6$ phase (Figures 2d-2f). Two soluble Mg-bearing phases Mg_2Si and $\text{Al}_5\text{Cu}_2\text{Mg}_8\text{Si}_6$ may be expected in Al-11Si alloy in accordance with the magnesium content. Since Mg_2Si was not revealed in the microstructure of the cast specimens of Al-11Si alloy, it could be stated that magnesium which was not dissolved in the α -Al phase

formed $\text{Al}_5\text{Cu}_2\text{Mg}_8\text{Si}_6$ phase with copper. The high magnesium content in the alloy (1.1 %) led to the precipitation of an $\text{Al}_5\text{Cu}_2\text{Mg}_8\text{Si}_6$ in the amount, which presents almost 32 % of all the intermetallic phases. Although the particles of $\text{Al}_5\text{Cu}_2\text{Mg}_8\text{Si}_6$ phase are hard to dissolve, they contribute to the strengthening of the alloy. A small quantity of Al_2Cu phase was detected in the fine mixture with $\text{Al}_5\text{Cu}_2\text{Mg}_8\text{Si}_6$, α -Al phase and eutectic silicon (Figure 2e), which is probably the result of the ternary eutectic reaction (α -Al + Al_2Cu + Si) or quaternary eutectic reaction (α -Al + Al_2Cu + $\text{Al}_5\text{Cu}_2\text{Mg}_8\text{Si}_6$ + Si). Furthermore, copper created compact or rod-shaped particles of AlCuFeNi phase (Figures 2e and 2f). Hence, the appearance of iron-based phase which bonded copper decreased its strengthening effect. Most of the nickel was found in the form of Al_3Ni phase, but tiny needle-shaped particles of Al_3FeNi were also recognised. The Al_3Ni phase was found to be 3.04 vol. %, accounting for 38.14 % of the total amount of intermetallic phases.

Two iron-bearing phases were also revealed as needle-shaped β - $\text{Al}_5\text{FeSi}(\text{Mn})$ phase (Figures 2d and 2f) and Chinese script shaped α - $\text{Al}_{15}(\text{Fe},\text{Mn},\text{Cu})_3\text{Si}_2$ phase (Figures 2c, 2e and 2f). In the surface area of the as-cast specimens of Al-11Si alloy, α - $\text{Al}_{15}(\text{Fe},\text{Mn})_3\text{Si}_2$ phase which may dissolve copper was discovered as an almost triple quantity of β - $\text{Al}_5\text{FeSi}(\text{Mn})$. The amount of manganese equal to one half of iron content, generally desirable from the standpoint of the transformation of β - Al_5FeSi to α - $\text{Al}_{15}(\text{Fe},\text{Mn})_3\text{Si}_2$ [41], was not achieved for the examined alloys. However, the appearance of α - $\text{Al}_{15}(\text{Fe},\text{Mn},\text{Cu})_3\text{Si}_2$ phase may be the result of the influence of other elements which were added for the correction of the harmful effect of the iron.

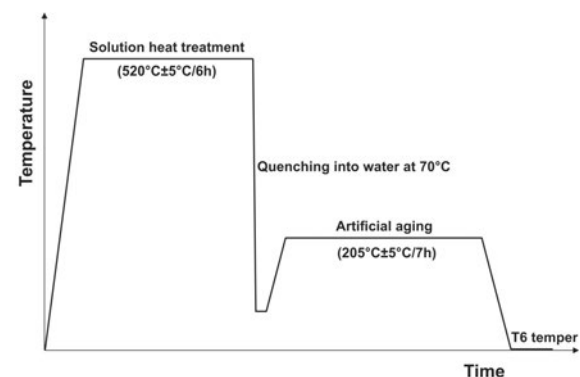


Figure 1. The temperature-time scheme of the T6 heat treatment procedure

Table 1. Chemical composition of examined alloys

Alloys	Element / wt.%									
	Si	Cu	Mg	Ni	Fe	Co	Mo	Mn	Sr	Al
Al-11Si	10.93	1.1	1.01	0.67	0.52	0.8	0.2	0.12	0.048	Bal.
Al-12.5Si	12.5	1.3	0.8	0.58	0.43	0.85	0.5	0.18	0.043	Bal.



Table 2. Quantity of phases (vol. %) in as-cast and T6-treated specimens

Phase	Quantity of phases / vol. %			
	As-cast specimens		T6-treated specimens	
	Al-11Si	Al-12.5Si	Al-11Si	Al-12.5Si
Primary Si	-	3.35	-	+
Eutectic Si	21.27	22.62	13.75	22.72
Al ₃ (Fe,Mn,Cu,Ni,Co)	-	2.09	-	3.17
α -Al ₁₅ (Fe,Mn,Cu) ₃ Si ₂	0.65	0.04	0.11	-
AlCuFeNi	1.16	-	-	-
Al ₅ Cu ₂ Mg ₈ Si ₆	2.51	1.92	1.85	1.06
Al ₂ Cu	0.31	0.09	-	-
Al ₃ Ni	3.04	3.9	3.02	4.49
β -Al ₅ FeSi(Mn)	0.24	0.16	0.27	0.13
Al ₉ FeNi	0.06	0.18	-	+

Molybdenum and cobalt moved equilibrium towards the formation of α -Al₁₅(Fe,Mn,Cu)₃Si₂ phase, but because of the conditions of crystallization that favour the appearance of β -Al₅FeSi(Mn) phase, all iron was not bounded in the phase of more favourable form.

Hypereutectic microstructure of as-cast Al-12.5Si alloy is shown in Figure 4. Around 3.35 vol. % of primary silicon, 22.62 vol. % of eutectic silicon and 65.65 vol. of α -Al phase were detected in as-cast samples of Al-12.5Si alloy (Table 2). Polyhedral crystals of the primary silicon are dominantly formed in the central part of the cross-section of the as-cast specimen close to the porosity, while narrow zones with dendrites of α -Al solid solution within eutectics could be recognised. Total amount of several intermetallic phases was 8.38 vol. %. Modified eutectic crystals coarser (Figures 4a, 4b and 4c) than in Al-11Si alloy are mostly present in the very fine mixture with Al₅Cu₂Mg₈Si₆ phase (Figures 4d and 4e). Lower quantity of Al₅Cu₂Mg₈Si₆ phase in Al-12.5Si alloy than in Al-11Si is caused by the magnesium content of about 0.8 %. The phase AlCuFeNi was not revealed in the microstructure of as-cast specimens of Al-12.5Si alloy. Compared to Al-11Si, a higher quantity of copper-bearing phases is expected in Al-12.5Si alloy since it contains more copper (1.3 %). However, the formation of a small quantity of Al₂Cu was detected (Figure 4e). Hence, the excess of copper should be discovered within some other phase. Definitely, it created large, star-like crystals or regular polygonal crystals of Al₃(Fe,Mn,Cu,Ni,Co) phase in an amount of 2.09 % which were observed as aggregates (Figures 4d and 4e) and often accompanied by the primary silicon crystals (Figure 4c). The high content of molybdenum and cobalt decreased the deleterious

effect of iron. However, iron formed needle-like β -Al₅FeSi(Mn) phase (Figure 4d) as well as Al₉FeNi which is most often seen with a massive compact iron-bearing phase (Figures 4c and 4d) and fine rounded particles of Al₃Ni phase (Figures 4d and 4e). Particles of α -Al₁₅(Fe,Mn,Cu)₃Si₂ phase could be recognised in small quantity.

After performing the T6 treatment, a small quantity of α -Al₁₅(Fe,Mn,Cu)₃Si₂ phase was observed in the specimens of Al-11Si alloy. Rounded eutectic silicon is interdendritic, distributed as could be seen in Figures 6a and 6b. It suggests that purely eutectic zones are not observed in as-cast specimens of Al-11Si alloy. Hence, the amount of eutectic silicon in T6-treated specimens is lower compared to as-cast specimens of Al-11Si alloy. While AlCuFeNi phase was not found, small rounded particles of copper-bearing phases Al₅Cu₂Mg₈Si₆ and Al₂Cu were revealed in T6-treated specimens of Al-11Si alloy (Figures 6c and 6d) in quantity lower by 0.97 vol. % compared to as-cast samples. Platelets of β -Al₅FeSi(Mn) phase and massive coagulated particles of Al₃Ni in aggregates with eutectic silicon and Al₅Cu₂Mg₈Si₆ were also observed (Figures 6c and 6d). Al₃Ni phase was revealed in the amount of 3.02 vol. % which is more than half of the total quantity of detected intermetallic phases.

In the microstructure of T6-treated samples of Al-12.5Si alloy, large, compact and rounded primary silicon crystals were rarely seen, but predominantly in surface area (Figures 7a and 7c), whereas eutectic silicon was rounded and mostly spheroidal (Figures 7c and 7d). Massive, compact star-like crystals of Al₃(Fe,Mn,Cu,Ni,Co) phase (Figures 7a, 7c and 7d) are revealed in 1.5 times greater quantity than in as-cast specimens. Short needles of Al₉FeNi phase (Figure 7d), fine rounded particles of Al₃Ni (Fig. 7d) and acicular β -



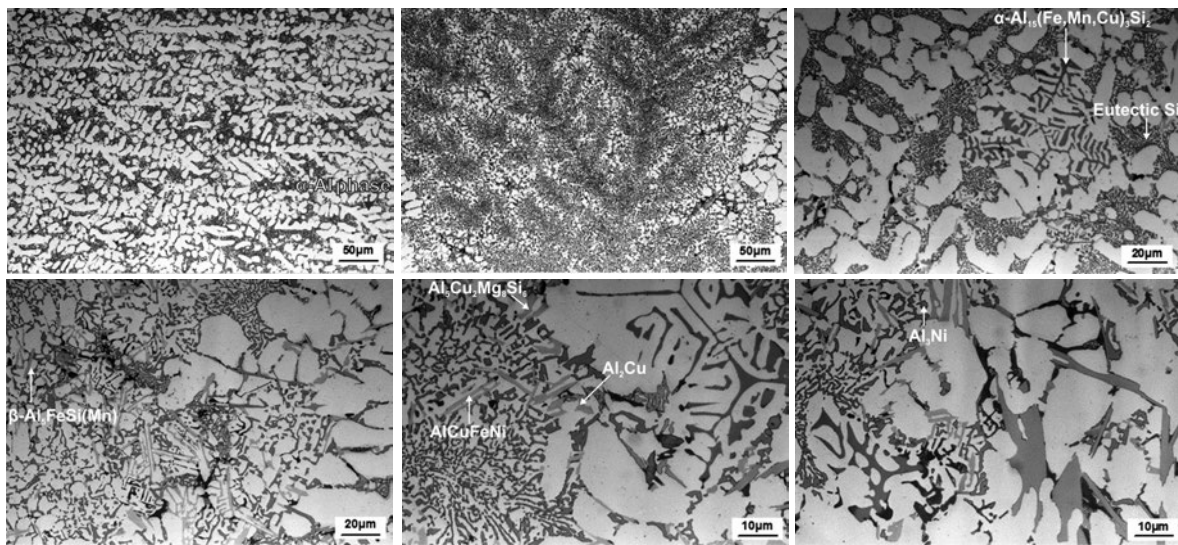


Figure 2. The microstructure of as-cast Al-11Si alloy at the surface of the specimen (a), central part of the specimen's cross-section (b), as well as other positions of examination (c) – (f)

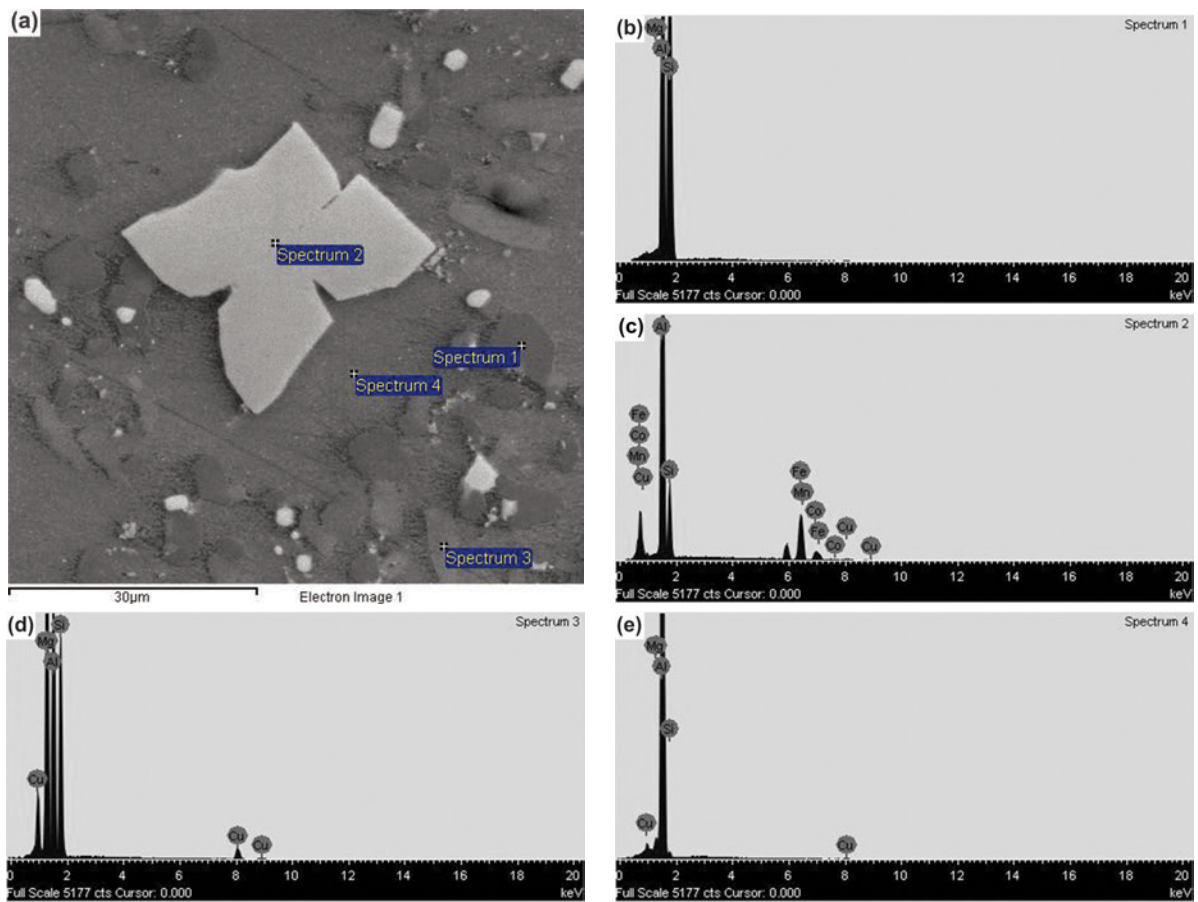


Figure 3. SEM image of phases (a) and corresponding EDS spectra from phases in as-cast samples of Al-11Si alloy (b – e)

Al₅FeSi(Mn) phase (Figure 7c) are also found in heat-treated specimens of the Al-12.5Si alloy. The copper-bearing phases are dissolved, and hence the quantity of Al₅Cu₂Mg₈Si₆ phase was decreased

compared to cast specimens of Al-12.5Si alloy. Al₂Cu phase was dissolved during solution treatment, while β-Al₅FeSi(Mn) phase was almost unaffected by T6 heat treatment in both alloys.



Taylor [43] was found that α and β phases in Al-Si alloys undergo to transformation, spheroidisation and Oswald ripening with the increase in the

solution treatment time, while only little signs of phase transformations were observed at the typical solution treatment temperature of about 540 °C.

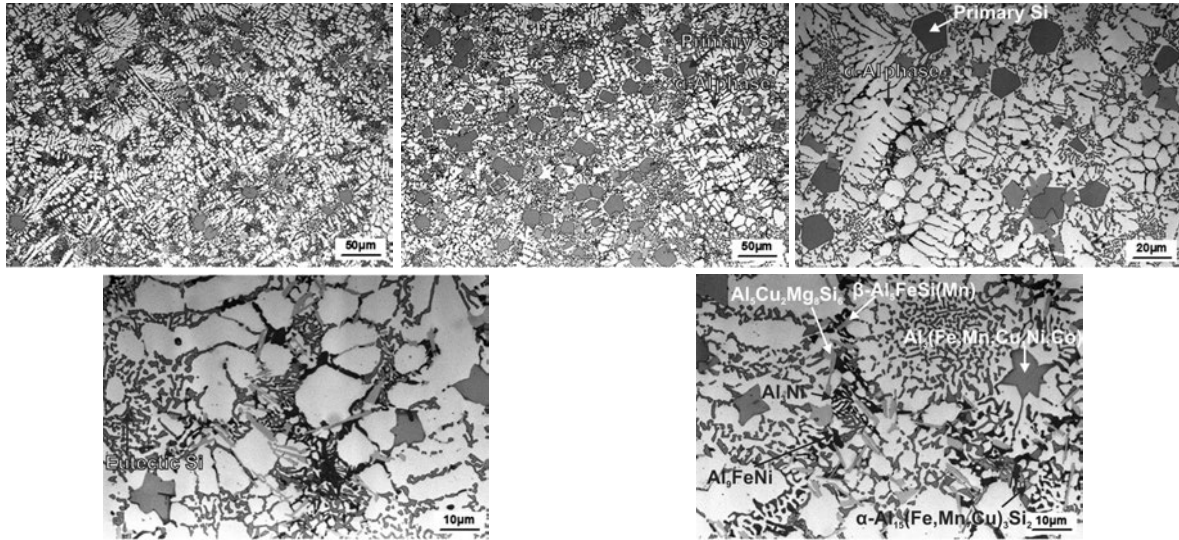


Figure 4. The microstructure of as-cast Al-12.5Si alloy at the surface of the specimen (a), and central part of the specimen's cross-section (b), as well as other positions of examination (c) – (e)

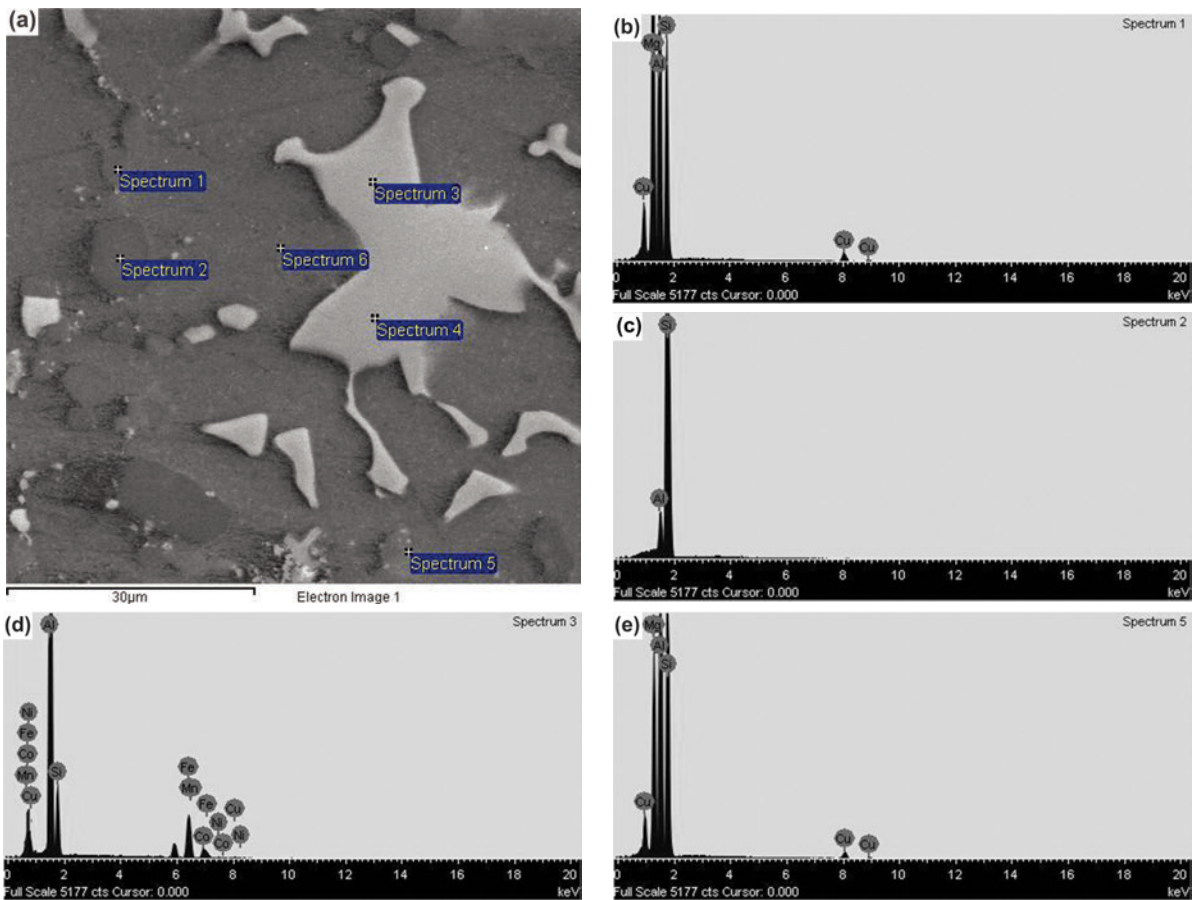


Figure 5. SEM image of phases (a) and corresponding EDS spectra from phases in as-cast samples of Al-12.5Si alloy (b – e)



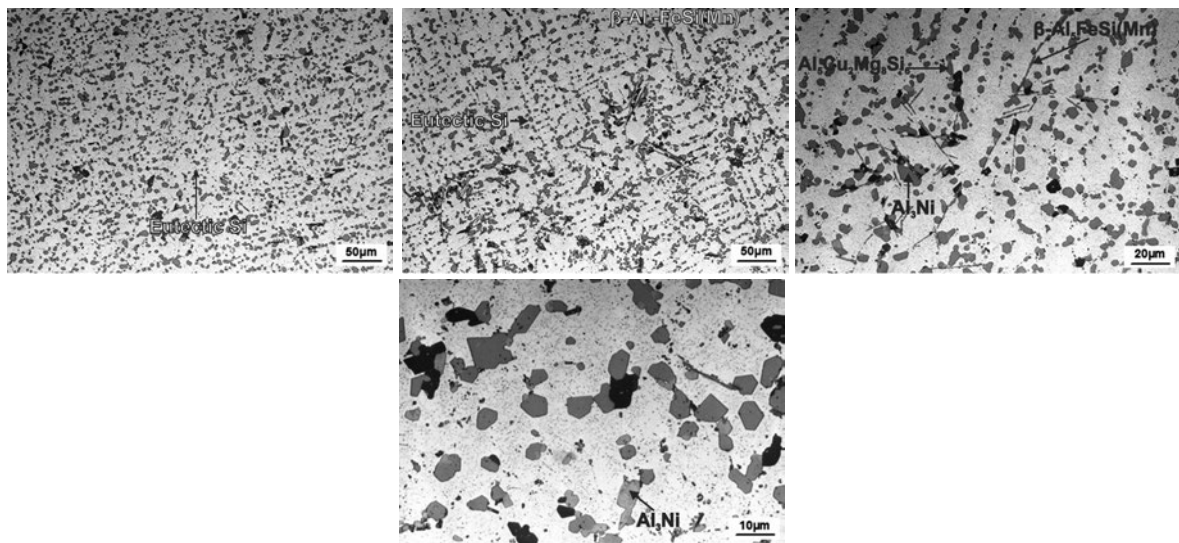


Figure 6. The microstructure of T6-treated Al-11Si alloy at the surface of the specimen (a), central part of the specimen's cross-section (b), as well as other positions of examination (c-d)

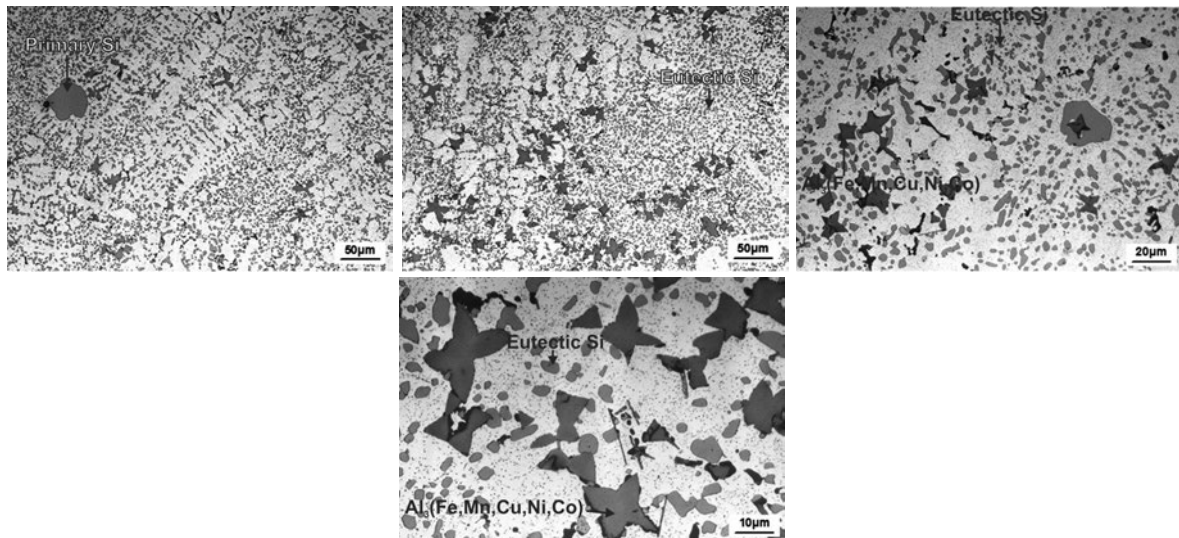


Figure 7. The microstructure of T6-treated Al-12.5Si alloy at the surface of the specimen, (a) and central part of the specimen's cross-section (b), as well as other positions of examination (c-d)

3.2. Mechanical properties

Table 3 lists the mechanical properties of as-cast and T6-treated specimens of the examined alloys which are the result of the intermetallic phase composition, the presence of α -Al dendrites, morphology of eutectic and primary silicon as well as the central porosity appearance.

While similar values of hardness were identified for both alloys, higher values of tensile strength and elongation were exhibited by samples of Al-11Si compared to Al-12.5Si alloy. Magnesium and copper formed $\text{Al}_5\text{Cu}_2\text{Mg}_8\text{Si}_6$ phase which was hard to dissolve. The particles of $\text{Al}_5\text{Cu}_2\text{Mg}_8\text{Si}_6$ and Al_2Cu phases promoted the tensile properties of both alloys.

The Al_3Ni phase was detected at least as one-third of the total amount of the intermetallic phases in examined specimens. The presence of larger particles of eutectic silicon in Al-12.5Si than in Al-11Si alloy may be considered as one of the causes of its lower tensile properties due to the creation of high levels of stress concentration [23]. It is worth to mention that hypereutectic Al-12.5Si alloy contained polyhedral crystals of primary silicon in as-cast specimens which were rarely seen after performing the T6 heat treatment. Those crystals certainly influenced the level of mechanical properties of Al-12.5Si alloy. In addition, intermetallic phases based on iron formed in all the samples (Figures 2 and 4) had deleterious effects on their mechanical properties, but nickel and

Table 3. Mechanical properties of as-cast and T6-treated specimens

Alloy	As-cast samples			T6-treated samples		
	R _m / MPa	Brinell Hardness / HB	Elongation / %	R _m / MPa	Brinell Hardness / HB	Elongation / %
Al-11Si	228.8	118	2.4	232.1	97	2.6
Al-12.5Si	192.5	121	0.8	226	104	2.3

cobalt mitigated that influence to some extent. The iron-bearing phase $\alpha\text{-Al}_{15}(\text{Fe},\text{Mn},\text{Cu})_3\text{Si}_2$ was revealed in higher quantity than needle-like $\beta\text{-Al}_5\text{FeSi}(\text{Mn})$ in as-cast specimens of alloy Al-11Si which contained 0.52 % of iron, 0.67 % of nickel, 0.80 % of cobalt, and 0.20 % of molybdenum. On the other hand, a small quantity of $\alpha\text{-Al}_{15}(\text{Fe},\text{Mn},\text{Cu})_3\text{Si}_2$ and $\beta\text{-Al}_5\text{FeSi}(\text{Mn})$ phases was detected in as-cast Al-12.5Si alloy containing 0.43 % of iron, 0.58 % of nickel, 0.85 % of cobalt, and 0.50 % of molybdenum. Besides, needle-like $\beta\text{-Al}_5\text{FeSi}(\text{Mn})$ and Al_9FeNi phase were also revealed in all the samples. The air and gasses entrainment during the filling phase probably caused the porosity observed in as-cast samples of Al-11Si and Al-12.5Si alloys. Dinnis et al. argued that the iron content contributes to the increase in the porosity level, but depending on silicon and copper concentration in alloy [42]. In order to avoid a decrease in mechanical properties, an increase in the porosity level and loss of ductility, the concentration of iron (in wt. %) in Al-Si alloys should be kept below the critical iron content that can be calculated [43] as follows:

$$Fe_{crit} \approx 0.075 \cdot [\text{wt.}\%Si] - 0.05 \quad (1)$$

As regards our alloys, Fe_{crit} was determined as 0.77 % and 0.89 % for Al-11Si and Al-12.5 Si alloys, respectively. Since the content of iron was below the critical level, it could not be recognised as the major cause of the central porosity of the examined alloys. At the same time, the content of copper of about 3 %, which was defined as critical for the creation of microporosity, was not reached in our alloys. Therefore, it could be concluded that the pouring procedure contributed to the porosity appearance in the examined samples.

The as-cast specimens of Al-11Si and Al-12.5Si alloys exhibited a tensile strength of 228.8 MPa and 192.5 MPa and a low elongation of 2.4 % and 0.8 %, respectively. Compared to our alloys, Shivaprasad et al. reported better values of tensile stress of 237.0 MPa as well as a significantly higher elongation of 9.1% for Al-12Si alloy due to the refinement of grains and the modification of the eutectic silicon [10]. The values of tensile strength and hardness of our alloys are higher than Al-12Si-xCu-1Mg-1.78Ni ($x = 0, 1, 2, 3$ and 4) alloys studied by Pratheesh et al. [37] as well as Al-Si-Cu-Mg-Ni alloys with 10.5 %, 12 %, 18 %, and 24 % of silicon examined by Zeren [44]. Nevertheless, Al-Si-Cu-Mg-Ni alloys with 10.5 %, 12 %, 18 %, and 24 %

of silicon exhibited an elongation below 2.4 %, while the lowest value (about 0.5 %) was recorded for the alloy with the highest content of silicon (24 %) [44].

The tensile testing of T6-treated samples revealed an increase in the tensile strength and elongation as well as a decrease in the hardness of both alloys. While a negligible increase was recognised for Al-11Si alloy, the strength of Al-12.5Si alloy was improved by 33.5 MPa. That enhancing of strength was caused to a great extent to the distribution of rounded and spheroidal eutectic silicon. After performing T6 heat treatment, the elongation of Al-12.5Si alloy was improved from 0.8 % to 2.3 %, whereas the samples of Al-11Si alloy exhibited a slight increase in the elongation. The results of the hardness measurement indicated a decrease after performing T6 heat treatment which may be caused by a wide dispersion of eutectic silicon particles. According to Iskah et al. [45], the area of widely dispersed silicon particles that is available for distribution of the forces applied by indenter during hardness measuring is less compared to the area of the soft $\alpha\text{-Al}$ phase, resulting in lower values of sample hardness.

After the T6-treatment, our alloys had higher values of tensile strength and similar hardness compared to Al-12Si-xCu-1Mg-1.78Ni alloys without copper or containing 1 % and 4 % of copper [37]. However, for Al-12Si-xCu-1Mg-1.78Ni alloy with 3 % of copper, the tensile strength above 250 MPa and hardness above 120 BHN [37] were found, which was better than the values exhibited by our alloys. The values of the hardness of the T6-treated samples of Al-Si-Cu-Mg-Ni alloys with 10.5 % and 12 % of silicon [44] and our Al-11Si and Al-12.5 Si alloys were similar. Same alloys have shown tensile strength of above 250 MPa [44] which was better compared to our specimens. However, the increase in silicon content in Al-Si-Cu-Mg-Ni alloys up to 18.1 % and 24.0 % contributed to a higher hardness (above 104 BHN), but a lower tensile strength (below 200 MPa) compared to our alloys [44].

3.3. Fracture analysis

Fracture surfaces of the as-cast and T6-treated Al-11Si and Al-12.5Si alloys are shown in Figures 8 to 13. The plane surface was observed indicating a brittle fracture (Figures 8, 10a, 10b, 11a, 11b, and 13a). However, the examination under higher magnification revealed predominantly intercrystalline fracture with the features of ductile failure in some areas.



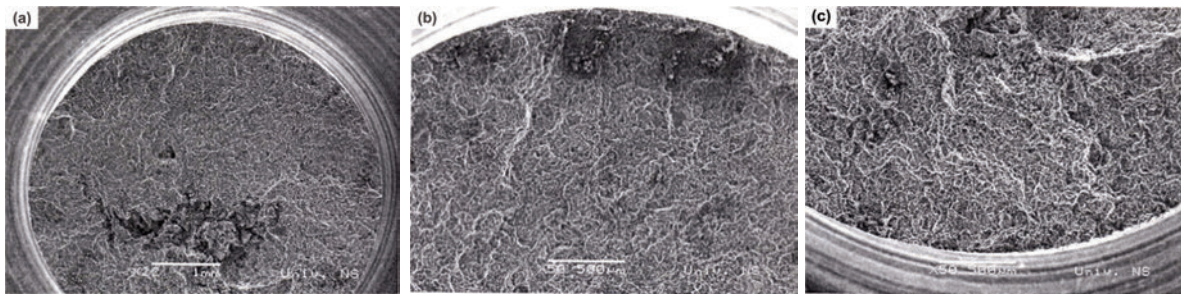


Figure 8. Fracture surfaces of as-cast specimens of alloy Al-11Si alloy

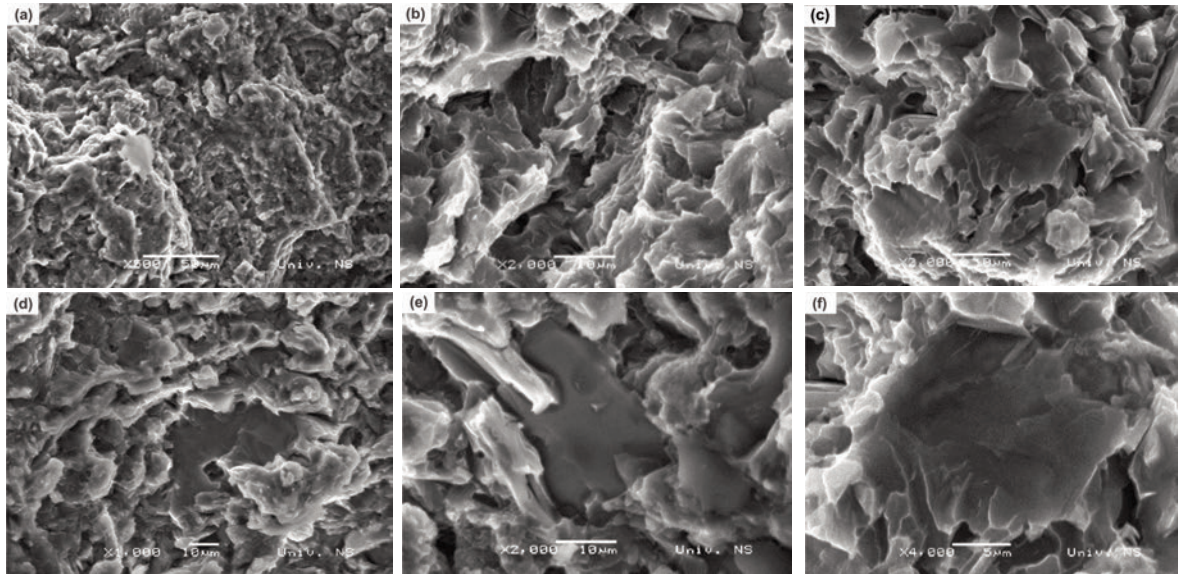


Figure 9. Fracture surface morphologies of as-cast specimens of Al-11Si alloy

The fracture of as-cast Al-11Si alloy is predominantly brittle as can be seen in Figures 9a and 9b. Smooth, flat surfaces of massive particles of intermetallic phases indicate the appearance of the intercrystalline fracture (Figures 9c, 9d, 9e, and 9f). The cracks were formed by the decohesion mechanism between the particles of the intermetallic phase/ α -Al solid solution rather than by the initiation of microcracks within the particles. When we consider elongated crystals, it can be concluded that microcracks are formed on the boundary surface of the particles and α -Al solid solution and spread through the long axis of the particle (Figure 9c) followed by the sideways spread and finally to fracture of the particles (Figure 9e). In the case of phase α - $\text{Al}_{15}(\text{Fe},\text{Mn},\text{Cu})_3\text{Si}_2$, the microcracks initiated on the boundary surface (Figure 9d) and spread along the branches of particles with Chinese script shape. Around the brittle particles of the intermetallic phase, shallow or deep dimples appeared, indicating ductile fracture of α -Al matrix as well as the increased resistance of eutectic silicon crystals to fracture. The dimple

areas are larger after the T6 heat treatment (Figure 10). Due to the rounding and coarsening of eutectic silicon crystals, the dimples are broader and deeper and mostly polygonal in shape. Microcracks occurred at the surface boundary of the intermetallic phase/ α -Al solid solution, but also due to the fracture of particles of the intermetallic phase without expanding into the surrounding α -Al solid solution. The appearance of the primary silicon crystals and, to a lesser extent, modified eutectic silicon crystals in the as-cast specimen of Al-12.5Si alloy (Figures 11a and 11b), contributed to a greater brittleness compared to the cast Al-11Si alloy. The microcracks were formed by a fracture of the primary silicon crystals (Figures 11d and 11e) and massive particles of star-like and polyhedron forms of $\text{Al}_3(\text{Fe},\text{Mn},\text{Cu},\text{Ni},\text{Co})$ phase (Figures 11f, 12a, 12b, and 12c). However, it should be noted that $\text{Al}_3(\text{Fe},\text{Mn},\text{Cu},\text{Ni},\text{Co})$ phase exhibited high resistance to fracture. Areas of ductile fracture were observed with tiny polygonal dimples (Figures 11c, 11f. and 11a), while in other places, the elongated dimples with a planar, shallow

bottom covering the width of the eutectic silicon lamellas were discovered (Figures 11e and 12c). When we consider the tensile testing of the alloys it should be kept in mind that the cracking initiation is affected by a very pronounced porosity, which is observed macroscopically for all the specimens. The pores in the central part of the sample's cross-section are deep and irregular in shape (Figures 8a, 10a, 10b, and 10c). However, there are also planar, more rounded pores (Figures 11a, 13a, and 13c) where the dendrites of the α -Al solid solution can be clearly seen (Figure 10b).

A higher ductility of the Al-12.5Si alloy is produced by the T6 heat treating (Figure 13c), which

is manifested in a larger area with polygonal dimples of different sizes (Figures 13b and 13d). Finer dimples were observed on the fracture surface of the T6 heat-treated samples of Al-12.5Si compared to Al-11Si alloy. This is in agreement with the size of the rounded crystals of eutectic silicon in the structure of these two heat-treated alloys. However, the increase in the fraction of ductile fracture has also been caused by the appearance of few primary silicon crystals, which are easily broken (Figure 13e). Although massive compact particles with iron recognised in the structure contribute to the brittle intercrystalline fracture, microcracks initiated in them are less visible (Figures 13d and 13f).

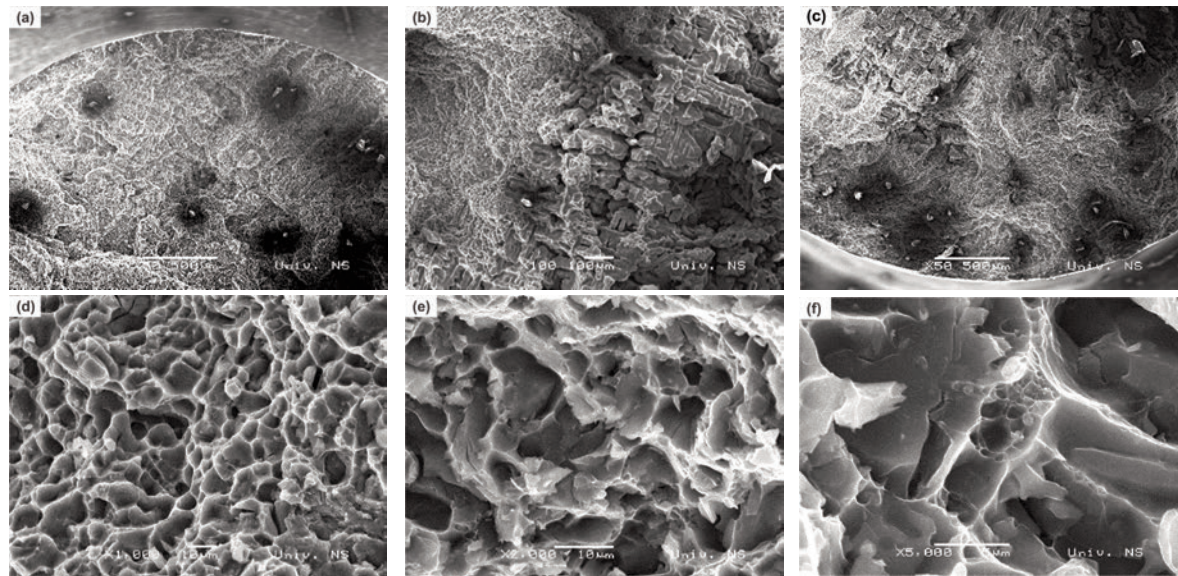


Figure 10. Fracture surface morphologies of T6-treated specimens of Al-11Si alloy

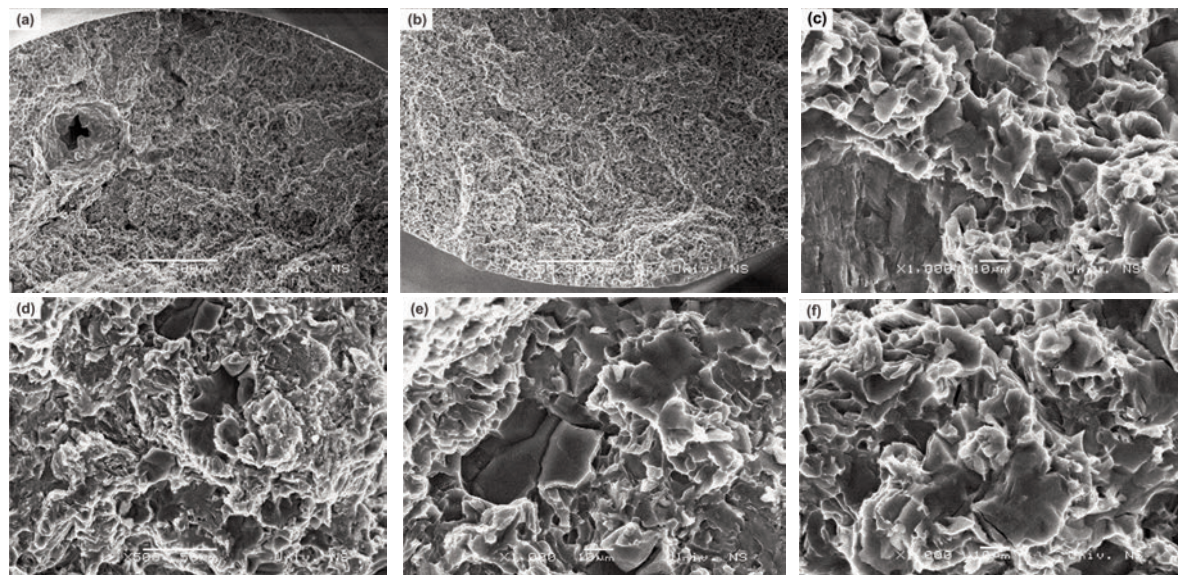


Figure 11. Fracture surface morphologies of as-cast specimens of Al-12.5Si alloy

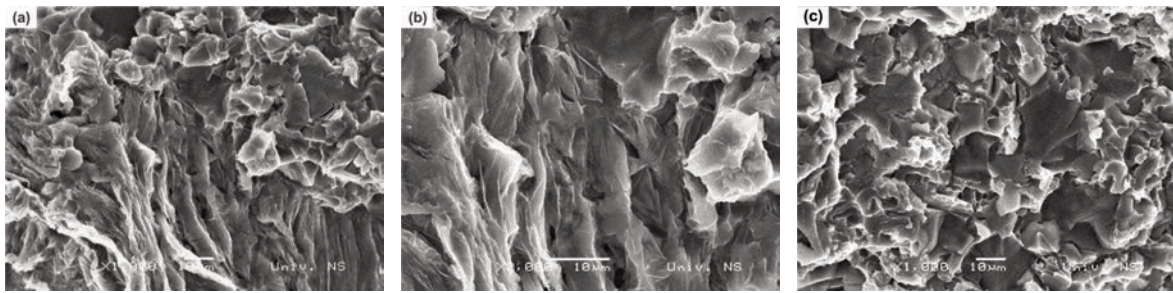


Figure 12. Fracture surface morphologies of as-cast specimens of Al-12.5Si alloy

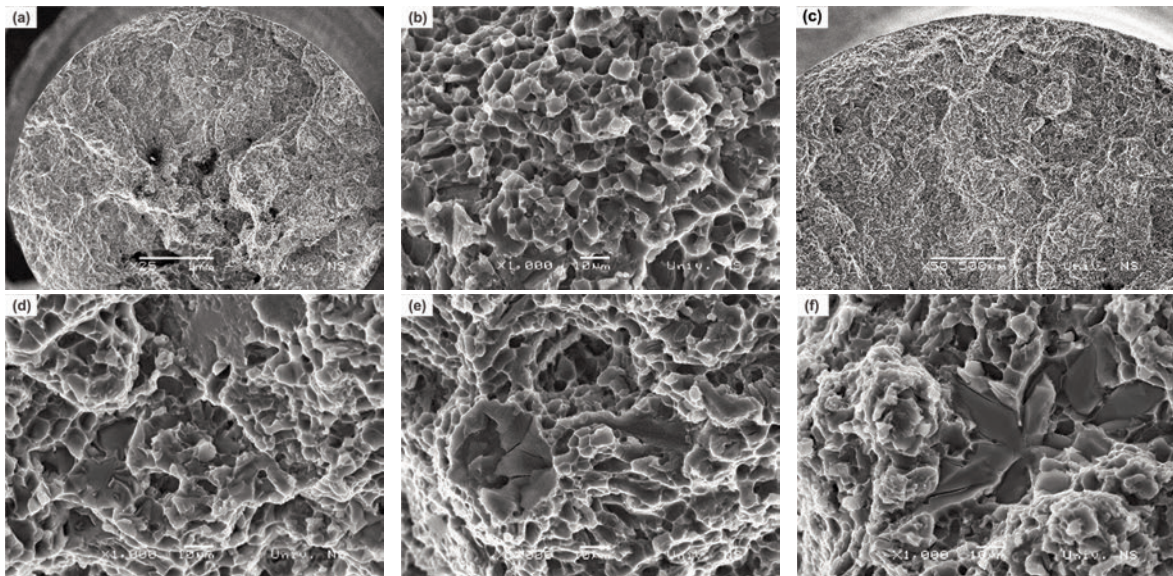


Figure 13. Fracture surface morphologies of T6-treated specimens of Al-12.5Si alloy

4. Conclusions

Eutectic silicon, α -Al dendrites, and several intermetallic phases such as α -Al₁₅(Fe,Mn,Cu)₃Si₂, Al₅Cu₂Mg₈Si₆, AlCuFeNi, Al₃Ni, Al₃FeNi, Al₃(Fe₂Mn,Cu,Ni,Co), Al₂Cu, and β -Al₅FeSi(Mn) were observed in the microstructure of hypoeutectic Al-11Si and hypereutectic Al-12.5Si alloys. Polyhedral crystals of primary silicon appeared in Al-12.5Si alloy.

The mechanical properties of both alloys were defined by the content of silicon, copper, magnesium, nickel, and iron. The samples of Al-11Si alloy exhibited higher values of tensile strength and elongation than Al-12.5Si alloy, while similar values of hardness were identified for both materials. Magnesium and copper formed Al₅Cu₂Mg₈Si₆ phase, which in addition to Al₂Cu phase promoted the tensile properties of both alloys. The one-third of the total amount of the intermetallic phases was observed as Al₃Ni phase. Lower values determined for Al-12.5Si compared to Al-11Si alloy were caused by the presence of larger particles of eutectic silicon, which created high levels of stress concentration. Besides,

the polyhedral crystals of primary silicon and intermetallic phases influenced the mechanical properties. Molybdenum and cobalt decreased the deleterious effect of iron.

The improvement of tensile strength and elongation after performing T6 heat treatment was only slight for samples of Al-11Si alloy. On the other side, compared to as-cast samples, the tensile strength of the T6-treated specimens of Al-12.5Si alloy was increased by 33.5 MPa, whereas the elongation was raised from 0.8 % to 2.3 %. The tensile properties were enhanced due to the distribution of rounded and spheroidal eutectic silicon. The decrease in the hardness values after the T6 heat treatment of both alloys, was probably caused by the wide dispersion of eutectic silicon particles.

The pronounced porosity affected the cracking initiation. However, the iron content in the examined alloys was not the primary cause of the central porosity. The massive particles of intermetallic phases indicated the intercrystalline fracture in Al-11Si alloy. On the other hand, silicon mainly in the form of primary crystals and in a lesser extent as eutectic crystals contributed to the brittle features in Al-12.5Si

alloy. The harmful effect of iron was decreased due to the addition of manganese, nickel, molybdenum and cobalt. The α -Al₁₅(Fe,Mn)₃Si₂ phase was discovered as an almost triple quantity of needle-shaped β -Al₅FeSi(Mn) phase.

Predominantly intercrystalline fracture with the features of ductile failure was recognised for both alloys. In as-cast specimens of Al-11Si alloy, the cracks were formed by the decohesion mechanism between the particles of intermetallic phase AlCuFeNi and α -Al solid solution. Shallow or deep dimples which appeared around the brittle particles of the intermetallic phase indicated a ductile fracture of α -Al matrix as well as the increased resistance of eutectic silicon crystals to fracture.

The primary silicon crystals mainly caused a high brittleness of as-cast Al-12.5Si alloy. The microcracks arose from the fracture of the primary silicon crystals and massive particles of the star-like and polyhedron forms of Al₃(Fe,Mn,Cu,Ni,Co) phase. Areas of ductile fracture were observed in some places with tiny polygonal dimples. Besides, the elongated dimples with a planar, shallow bottom covering the width of the eutectic silicon lamellas were revealed.

Large dimples areas appeared after the T6 heat treatment of the specimens of Al-11Si alloy. Microcracks occurred at the surface boundary of the intermetallic phase/ α -Al solid solution. Also, without expanding into the surrounding α -Al solid solution, the fracture of particles of the intermetallic phase influenced the fracture behaviour.

The T6 heat treating improved the ductility of the Al-12.5Si alloy. The increase in the fraction of ductile fracture was caused by the appearance of few easily broken primary silicon crystals. Despite the contribution of the massive compact particles with iron to the brittle intercrystalline fracture, microcracks initiated in them were less visible.

References

- [1] R. X. Li, R. D. Li, Y. H. Zhao, L. Z. He, C. H. Li, H. R. Guan, Z. Q. Hu, *Mater. Lett.*, 58 (15) (2004) 2096-2101.
- [2] L. Liu, A. M. A. Mohamed, A. M. Samuel, F. H. Samuel, H. W. Doty, S. Valtierra, *Metall. Trans. A*, 40A (10) (2009) 2457-2469.
- [3] M. Javidani, D. Larouche, *Int. Mater. Rev.*, 59 (3) (2014) 132-158.
- [4] V. S. Zolotarevsky, N. A. Belov, M. V. Glazoff, *Casting Aluminum Alloys*, 1st ed., Elsevier, Oxford, 2007, p. 328.
- [5] A. Ahmed, M. S. Wahab, A. A. Raus, K. Kamarudin, Q. Bakhsh, D. Ali, *Indian J. Sci. Technol.*, 9 (36) (2016) 1-7.
- [6] H. C. Liao, M. Zhang, J. J. Bi, K. Ding, X. Xi, S. Q. Wu, *J. Mater. Sci. Technol.*, 26 (12) (2010) 1089-1097.
- [7] M. M. Mansoor, I. Salam, A. Tauqir, *IOP Conf. Ser.: Mater. Sci. Eng.*, 146 (1) (2016) 1-6.
- [8] G. K. Sigworth, *Int. J. Metalcast.*, 2 (2) (2008) 19-40.
- [9] J. Jorstad, and D. Apelian, *Int. J. Metalcast.*, 3 (3) (2009) 13-33.
- [10] C. G. Shivaprasad, K. Aithal, S. Narendranath, V. Desai, P. G. Mukunda, *Int. J. Microstruct. Mater. Prop.*, 10 (3/4) (2015) 274-284.
- [11] K. Al-Helal, I. C. Stone, Z. Fan, *Trans. Indian Inst. Met.*, 65 (2012) 663-667.
- [12] X. F. Wu, G. A. Zhang, *J. Mater. Sci.*, 46 (22) (2011) 7319-7327.
- [13] F. C. Robles-Hernandez, J. M. H. Ramirez, R. Mackay, *Al-Si Alloys: Automotive, Aeronautical, and Aerospace Applications*, Springer, Cham, Switzerland, 2017, p. 4,7,9,10.
- [14] J. E. Hatch, *Aluminum: Properties and Physical Metallurgy*, American Society for Metals, Metals Park, Ohio, 1984, p. 226, 230, 234, 235.
- [15] G. Mrówka-Nowotnik, *Arch. Mater. Sci. Eng.*, 38 (2) (2009) 69-77.
- [16] D. K. Dwivedi, R. Sharma, A. Kumar, A., *Int. J. Cast. Metal. Res.*, 19 (5) (2006) 275-282.
- [17] Y. Han, A. M. Samuel, H. W. Doty, S. Valtierra, F. H. Samuel, *Mater. Des.*, 58 (2014) 426-438.
- [18] J. R. Davis, *Alloying: Understanding the Basics*, 1st ed., ASM International, Materials Park, 2001, p. 392.
- [19] J. G. Kaufman, E. L. Rooy, *Aluminum Alloy Castings: Properties, Processes, and Applications*, ASM International, Materials Park, 2004, p.16
- [20] M. Rejaeian, M. Karamouz, M. Emamy, M. Hajizamani, *Trans. Nonferrous Met. Soc. China*, 25 (11) (2015) 3539-3545.
- [21] Y. Wang, Y. Xiong, *Mat. Sci. Eng. A.*, 280 (2000) 124-127.
- [22] S. Farahany, A. Ourdjini, H. R. Bakhsheshi-Rad, *Trans. Nonferrous Met. Soc. China*, 26 (1) (2016) 28-38.
- [23] M. Karamouz, M. Azarbaras, M. Emamy, M. Alipour, *Mater. Sci. Eng. A.*, A582, (2013) 409-414.
- [24] Y. C. Tzeng, C. T. Wu, H. Y. Bor, J. L. Horng, M. L. Tsai, S. L. Lee, *Mater. Sci. Eng. A.*, 593 (2014) 103-110.
- [25] R. Wieszala, J. Piątkowski, *Arch. Foundry Eng.*, 17(4) (2017) 175-178.
- [26] G. H. Zhang, J. X. Zhang, B. C. Li, W. Cai, *Prog. Nat. Sci. Mater. Int.*, 21 (5) (2011) 380-385.
- [27] C. Y. Jeong, *Mater. Trans.*, 54 (4) (2013) 588-594.
- [28] G. Mrowka-Nowotnik, J. Sieniawski, *Arch. Mater. Sci. Eng.*, 47 (2) (2011) 85-94.
- [29] R. K. Singh, A. Telang, S. Das, *AJER*, 5(8) (2016) 133-137.
- [30] D. A. Lados, D. Apelian, *Metall. Mater. Trans. B.*, 42 (1) (2011) 171-180.
- [31] B. E. Slattery, T. Perry, A. Edrissy, *Mat. Sci. Eng. A*, 512 (2009) 76-81.
- [32] C. Xu, C. Wang, H. Yang, Z. Liu, H. Yamagata, C. Ma, *Mat. Sci. Forum*, 850 (2016) 594-602.
- [33] L. Chen, D. Wang, X. Che, F. Li, *China Foundry*, 9 (1) (2012) 39-42.
- [34] S. K. Shaha, F. Czerwinski, W. Kasprzak, J. Friedman, D. L. Chen, *J. Alloys Compd.* 615 (2014) 1019-1031.
- [35] T. S. Srivatsan, M. Al-Hajri, V. K. Vasudevan, *Int. J. Fatigue*, 27 (4) (2005) 357-371.



- [36] G. Rajaram, S. Kumaran, R. Srinivasa Rao, Mat. Sci. Eng. A, 528 (1) (2010) 247-253.
- [37] K. Pratheesh, A. Kanjirathinkal, M. A. Joseph, Int. Metalcast. 11 (4) (2017) 831-842.
- [38] P. Stoyanov, D. Linsler, T. Schlarb, M. Scherge, R. Schwaiger, J. Mater. Sci., 50 (16) (2015) 5524-5532.
- [39] X. F. Wu, G. A. Zhang, J. Mater. Sci., 46 (2011) 7319-7327.
- [40] E. Sjolander, S. Seifeddine, J. Mater. Process. Technol., 210 (2010) 1249-1259.
- [41] X. Cao, J. Campbell, Mater. Trans. JIM, 47 (5) (2006) 1303-1312.
- [42] C. M. Dinnis, J. A. Taylor, A. K. Dahle, Mater. Sci. Eng., 425 (2006) 286-296.
- [43] J. A. Taylor, Procedia Mater. Sci., 1 (2012) 19-33.
- [44] M. Zeren, Mater. Des., 28 (2007) 2511-2517.
- [45] M. Ishak, A. Amir, A. Hadi A., Proc. International Conference on Mechanical Engineering Research (ICMER2013); 2013 July 1-3; Bukit Gambang Resort City, Kuantan, Pahang, Mayasia, 2013, p. 01-14.

UTICAJ HEMIJSKOG SASTAVA I T6 TERMIČKOG TRETMANA NA MEHANIČKE OSOBINE I LOM Al-Si LEGURA ZA DELOVE MOTORA SA UNUTRAŠNIM SAGOREVANJEM

D. Vuksanović, V. Asanović, J. Šćepanović, D. Radonjić*

Univerzitet Crne Gore, Metalurško-tehnološki fakultet, Podgorica, Montenegro

Apstrakt

Mikrostrukturnim ispitivanjima Al-Si legura namenjenih za izradu komponenti motora sa unutrašnjim sagorevanjem otkriven je složeni fazni sastav u svim uzorcima. Pored dendrita α -čvrstog rastvora, eutektičkog silicijuma i nekoliko intermetalnih faza, identifikovanih u livenim uzorcima obe legure, poliedarski kristali primarnog silicijuma otkriveni su u Al-12.5Si leguri. Bolje zatezne osobine su utvrđene za uzorke od Al-11Si. Pretežno interkristalni lom sa područjima duktilnog karaktera je primećen kod obe legure. U livenim uzorcima od legure Al-11Si, šupljine su formirane mehanizmom dekohezije između čestica intermetalne faze AlCuFeNi i α -čvrstog rastvora. Mikropukotine inicirane na graničnoj površini širile su se duž grana čestica α -Al₁₅(Fe,Mn,Cu)₃Si₂. Nakon T6 tretmana Al-11Si legure, skoro polovinu ukupne količine intermetalnih faza činila je Al₃Ni faza, dok je zapažena mala količina faza na bazi gvožđa. Sferoidizirani eutektički silicijum, manja količina Al₅Cu₂Mg₈Si₆ i veća količina Al₃(Fe,Mn,Cu, Ni,Co) faze otkriveni su u termički obrađenim uzorcima od legure Al-12.5Si. Zaobljeni kristali eutektičkog silicijuma doprineli su poboljšanju njihovih zateznih osobina. Veće i dublje jamice uglavnom poligonalnog oblika zapažene su u uzorcima od legure Al-11Si nakon T6 tretmana. Mikropukotine su se javljale na graničnoj površini intermetalna faza/ α -čvrsti rastvor.

Ključne reči: Intermetalne faze; Mehaničke osobine; Lom

